Efficient calculation of electronic coupling integrals with the dimer projection method via a density matrix tight-binding potential

Efficient Calculation of Electronic Coupling Integrals with the Dimer Projection Method via a Density Matrix Tight-Binding Potential

J. T. Kohn,[1] N. Gildemeister,[2] S. Grimme,[1] D. Fazzi,[3, a)] and A. Hansen[1, b)]
[1)] *Mulliken Center for Theoretical Chemistry, University of Bonn, Beringstrasse 4, 53115 Bonn, Germany.*
[2)] *Department of Chemistry, Greinstrasse 4-6, 50939 Köln, Germany.*
[3)] *Dipartimento di Chimica "Giacomo Ciamician", Via Selmi 2, 40126 Bologna, Italy.*[c)]

(*Electronic mail: hansen@thch.uni-bonn.de)

(*Electronic mail: daniele.fazzi@unibo.it)

(Dated: 22 February 2024)

Designing organic semiconductors for practical applications in organic solar cells (OSCs), organic field-effect transistors (OFETs), and organic light-emitting diodes (OLEDs) requires understanding charge transfer mechanisms across different length and time scales. The underlying electron transfer (ET) mechanisms can be efficiently explored using semiempirical quantum mechanical methods (SQM). The dimer projection method (DIPRO) combined with the recently introduced non-selfconsistent density matrix tight-binding potential (PTB [Grimme *et al., J. Chem. Phys.,* 2023, **158**.]) is used in this study to evaluate charge transfer integrals important for understanding charge transport mechanisms. PTB, parameterized for the entire periodic table up to Z=86, incorporates approximate non-local exchange, allowing efficient and accurate calculations for large hetero-organic compounds. Benchmarking against established databases such as Blumberger's HAB sets, or our newly introduced JAB69 set, and comparing with high-level reference data from ωB97X-D4 calculations confirms that DIRPO@PTB consistently performs well among the tested SQM approaches for calculating coupling integrals. DIPRO@PTB yields reasonably accurate results at low computational cost, making it suitable for screening applications and applications to large systems such as metal-organic frameworks (MOFs) and cyanine-based molecular aggregates further discussed in this work.

I. INTRODUCTION

To develop new functional semiconducting materials for opto-electronic applications, a comprehensive understanding of the electron transfer mechanisms is indispensable. Electron transfer processes are subject to extensive computational studies since the early 1970s and are still a strongly evolving topic.[1] Today, semiempirical methods (SQM) enable the investigation of reasonably large systems to test their suitability for high-performance conductive materials.[2] This is especially important for the design of molecular and polymeric organic semiconductors, with increasing application in organic solar cells (OSCs),[3] organic field effect transistors (OFETs),[4] organic light-emitting diodes (OLEDs),[5] and other organic electronics (OEs).[6–8] In contrast to metallic conductors, that exhibit band transport, organic semiconductors mostly exhibit different variations of hopping transport.[9,10] Researchers have developed various methods to measure and model electron and hole mobilities in recent years[11–13]. The most common approaches utilize Marcus' theory and subsequently employ Monte Carlo simulations to evaluate the charge mobility[14–17]. In this approach, the first step involves calculating electron transfer integrals, also known as coupling integrals (H_{ab} or J_{ab}), between different fragments or localized states. Fragmentation of the investigated chemical space can be carried out using a wide range of theories, most of which can be combined with any available orbital localization method[18]. Several methods for calculating coupling integrals exist, including charge constrained density functional theory (CDFT)[19], fragment orbital DFT (FODFT) or fragment orbital density functional tight binding (FODFTB)[20], projection-operator diabatization (POD)[21–23], frozen density embedding (FDE)[24], generalized Mulliken-Hush (GMH)[25], multistate DFT (MSDFT)[26], analytic overlap method (AOM)[27], machine-learning approaches (ML)[28,29], and the dimer projection method (DIPRO)[30].

Compounds for OE are often many hundreds of atoms large, have complicated intra- and intermolecular structure, or exhibit a wide conformational variety making the exploration of all three-dimensional coupling possibilities, charge carrier pathways, and their corresponding integrals time-consuming. Additionally, for charge mobility calculations in solids, either crystalline or amorphous, thermal fluctuations have to be accounted for. To achieve that, extensive molecular dynamic simulations (MDs) are required and coupling integrals are evaluated several thousands to tens of thousands of times along a single trajectory. By using SQM, computation times can be significantly reduced while still reasonably accurate results can be obtained, enabling large length- and time-scale investigations such as those involving DNA[31,32], complex fullerene-based acceptors for organic photovoltaics (OPV) applications[33], materials design and screening for new OE compounds[34], impact of thermal disorder effects on charge mobility[35], charge transport in covalent organic frameworks[36], pietzo effect[37], and polymer crystals[38] to become feasible. The advantages of DIPRO compared to other coupling integral methods is that it is a post-processing

[a)] https://www.unibo.it/sitoweb/daniele.fazzi/en
[b)] https://www.chemie.uni-bonn.de/grimme/de
[c)] ‡*correspondingauthor*

method and can in principle be used with any existing code and mean-field theory level. Furthermore, the mathematics behind DIPRO are easily understandable, accessible, and implementable.

In the following, we use the recently introduced semiempirical non-selfconsistent tight-binding potential PTB[39] together with DIPRO to calculate coupling integrals for a wide range of hetero-organic compounds. We transfer our approach to the investigation of challenging systems such as merocyanines, whose resonant electronic structure remains challenging due to their strong intramolecular charge transfer, and large metal-organic frameworks (MOFs), that due to their extended and highly delocalized structure are computationally demanding. We benchmark the results against ωB97X-D4/TZ2P reference DFT data and compare them to other SQM methods using common benchmarks such as Blumberger's HAB7[40] , HAB11[41] , and HAB79[42] sets.

II. THEORY

The dimer projection method, known as DIPRO[30] , enables the calculation of the coupling integrals between pairs of molecules. DIPRO necessitates three quantum mechanical single-point calculations from any source (e.g., SQM, HF, DFT): one for each monomer (A,B) and another for the dimer (AB). The relevant equations are provided below:

$$\gamma_1^i = \mathbf{C_A}^i \cdot \mathbf{S_{AB}} \cdot \mathbf{C_{AB}} \tag{1}$$

$$\gamma_2^j = \mathbf{C_B}^j \cdot \mathbf{S_{AB}} \cdot \mathbf{C_{AB}} \tag{2}$$

$$S_{ab}^{ij} = \gamma_1^i \cdot \gamma_2^j \tag{3}$$

$$J_{ab}^{ij} = \gamma_1^i \cdot \mathbf{E_{AB}} \cdot \gamma_2^j \tag{4}$$

$$J_{ab,eff}^{ij} = \left| \frac{J_{ab}^{ij} - 0.5 \cdot (E_A^i + E_B^j) \cdot S_{ab}^{ij}}{1 - (S_{ab}^{ij})^2} \right|. \tag{5}$$

Here, **C** are the orbital coefficients, **S** is the AO overlap matrix, **E** are the orbital energies, i and j denote the molecular orbitals that are considered for the electron or hole transfer. In this work, i and j always correspond to the HOMOs of the coupled molecules.

The DIPRO approach is limited, as it is not valid for very large overlaps (i.e., short intermolecular distances) or for $J_{ab}^{ij} \lessapprox 0.5 \cdot (E_A^i + E_B^j) \cdot S_{ab}^{ij}$ in the case of methodically strongly underestimated J_{ab}. One way to address the first limitation is by focusing solely on physically meaningful, i.e., equilibrium distances. The latter issue is commonly resolved by introducing method-specific scaling factors[42,43] . These aspects will be thoroughly discussed in Section V A .

The variation between different approaches for calculating coupling integrals is relatively small, typically around 1%, as long as the considered transfer states and orbitals are similar[42] . Thus, the desired accuracy of coupling integrals heavily relies on the chosen level of theory. Multi-reference configuration interaction (MRCI) and n-electron valence state perturbation theory (NEVPT2) are generally regarded as the "gold standard" for calculating coupling integrals[44] . Density functional theory (DFT) methods exhibit reduced accuracy along Jacob's ladder, with range-separated hybrids or hybrids with approximately 50% Fock exchange performing the best. Different implementations of the same functional can yield up to a 35 meV deviation in $J_{ab,eff}$, corresponding to a typical relative error of 10%. Moving down the ladder towards generalized gradient approximations (GGAs) results in an accuracy decrease of about 10% compared to RSH methods. Descending further to semiempirical methods leads to a deviation from the reference values in the range of 100 to 120 meV (around 40%)[45] . These trends are also depicted in Fig. S1 in the SI. However, this methodical deviation can be significantly reduced by applying a scaling factor to $J_{ab,eff}$, resulting in improvements of up to one order of magnitude.

III. FIT AND TEST SET

The co-planar dimers, with 3.5Å intermolecular distance, of the HAB79 benchmark by Blumberger *et. al.*[42] serve as a fit set to obtain the empirical scaling factors for the PTB coupling integrals. Here, we introduce a new test set called JAB69, that includes the HAB7[40] and HAB11[41] benchmarks and enhances it by 51 chemically comparable, but larger dimers.
The JAB69 benchmark consists of 69 mostly medium-sized, conjugated, parallel, planar, perfectly eclipsed-stacked, homo-dimers with a distance of 3.5Å between their centers of mass. The set is sorted by element composition, i.e., 20 purely carbon- and hydrogen-containing molecules (CH subset), 27 molecules that additionally contain nitrogen and oxygen (CHNO subset), 16 residues furthermore containing sulfur (CHONS subset), and 6 residues with other elements (CHNOSE subset). Fig. 1 depicts the Lewis structures of the monomers (optimized Cartesian coordinates are available in the Supporting Information (SI)).

IV. COMPUTATIONAL DETAILS

We computed coupling integrals at the ωB97X-D4/TZ2P,[46–48] PBE-D4/TZ2P,[49] PTB,[39] ZINDO[50] and DFTB3(3ob-3-1 parameter set)[51,52] levels of theory. We calculated PTB single points with the `ptb 3.7` standalone program[53] using a customized more verbose output and subsequent post-processing with the development version of our DIPRO in-house code.[54] ZINDO single points were calculated within `Gaussian16` program version C.01[55] followed by a custom DIPRO post-processing script.[56] ωB97X-D4, PBE-D4, and DFTB3 coupling integrals were

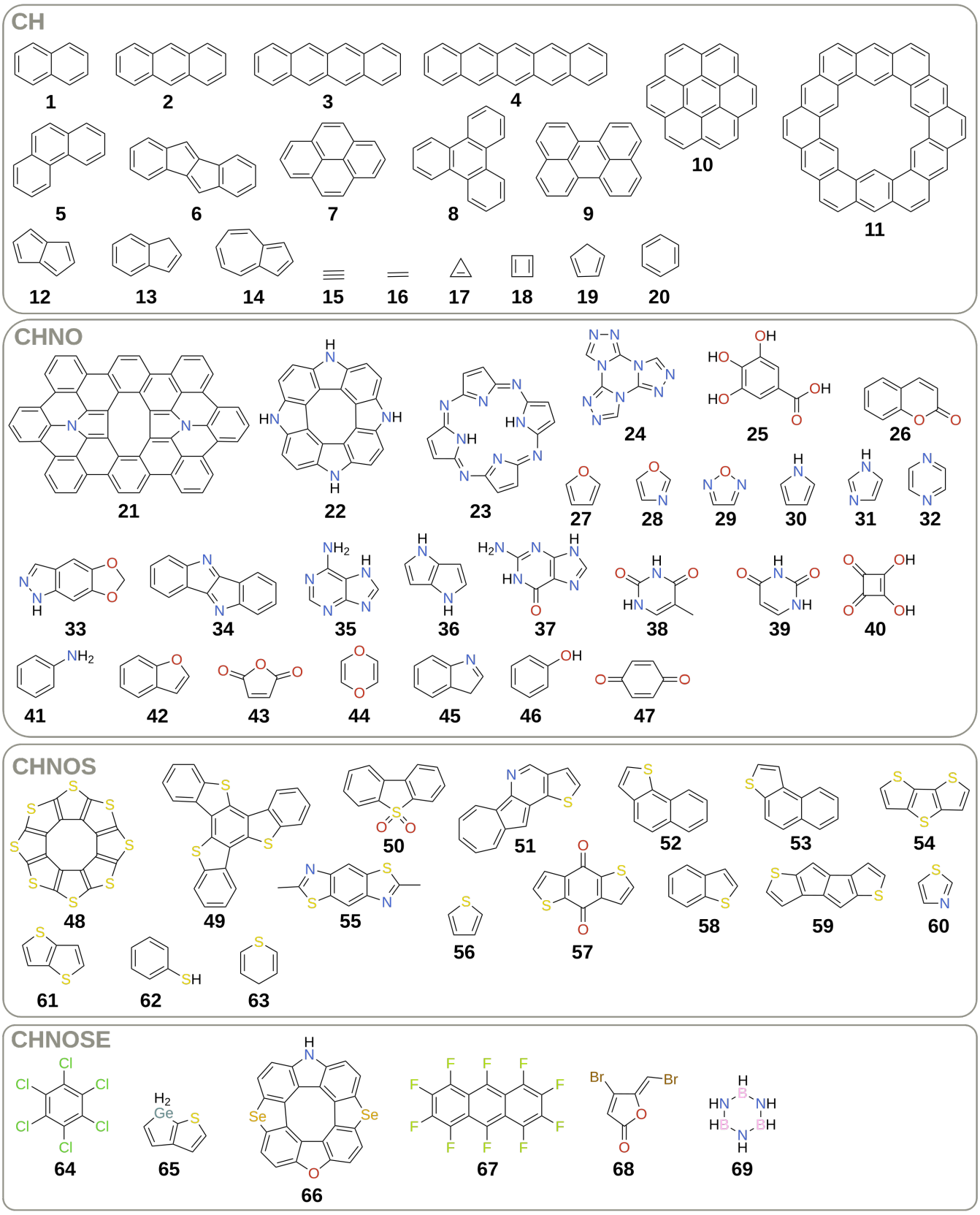

FIG. 1. Monomers of the JAB69 test set sorted by element composition.

calculated using AMS V.2020.102.[57,58] We took reference data and geometries for the HAB79 test set from Ref. 42, but used ωB97X-D4 references for both test sets, HAB79 and JAB69. The range separated hybrid ωB97X-D4/TZ2P proved to be robust and good performing and is widely used for the calculation of electronic coupling integrals for larger molecules as a kind of silver standard[42] .

For the statistical evaluation, we used the mean deviation (MD) and relative mean deviation (relMD), the mean absolute deviation (MAD) and relative mean absolute deviation (relMAD), the standard deviation (SD) and relative standard deviation (relSD), the Pearson correlation coefficient (ρ_P), and the Spearman rank coefficient (ρ_S). The respective equations are provided in the SI.

V. RESULTS

In general, coupling integrals calculated at the SQM level are smaller than at the DFT level. This is a direct consequence of the minimal basis set used by most SQM methods, thus leading to overlocalization of the coupled states and too fast exponential decay of $|J_{ab,eff}|$ with the distance. As PTB uses a larger vDZP basis set, this trend is less pronounced here compared to, e.g., GFN-xTB or ZINDO. Additionally, most SQM methods underestimate electronic gaps, which also directly affects the coupling. The DIPRO formula for $|J_{ab,eff}|$ (see eq. 5) exhibits some shortcomings (e.g., it is not valid for very large overlaps). This can be overcome by applying a uniform scaling factor f=1.921 to the PTB orbital energies of the dimer, according to the following equation:

$$\gamma_1^i \cdot (\mathbf{E_{AB}} \cdot f) \cdot \gamma_2^j = J_{ab}^{ij} \cdot f \tag{6}$$

$$J_{ab,eff}^{ij} = \left| \frac{J_{ab}^{ij} \cdot f - 0.5 \cdot (E_{mon1}^{i} + E_{mon2}^{j}) \cdot S_{ab}^{ij}}{1 - (S_{ab}^{ij})^2} \right| \tag{7}$$

The scaling factor f is determined by:

$$f = \frac{\sum_{i=1}^{n} |J_{ab}^{ij}(\omega B97X-D4)| / |J_{ab}^{ij}(method)|}{n} \tag{8}$$

whereas n denotes the total number of considered systems. We determined the scaling factor on the HAB79 set and then applied it to all other calculations. There are two drawbacks of this procedure. First, the scaling of all values leads to increased SD and RMSD compared to unscaled SQM methods. Second, the scaling can accidentally introduce huge errors and thus biases the statistical evaluation. Although, the calculated scaling factor is not overly sensitive to the underlying test set, it is sensitive to the elemental composition and the dimer distance. The transfer of this scaling factor to less common elements, especially metals and metalloids, is not encouraged. We advise to determine a new scaling factor for these special purposes. No such scaling factors were applied to the other methods, either because it was not necessary according to eq. 5, or because the chosen program package did not allow user intervention.

A. HAB79

Fig. 2 depicts the correlation between different SQM methods and ωB97X-D4/TZ2P reference coupling integrals J_{ab} for the HAB79 set.

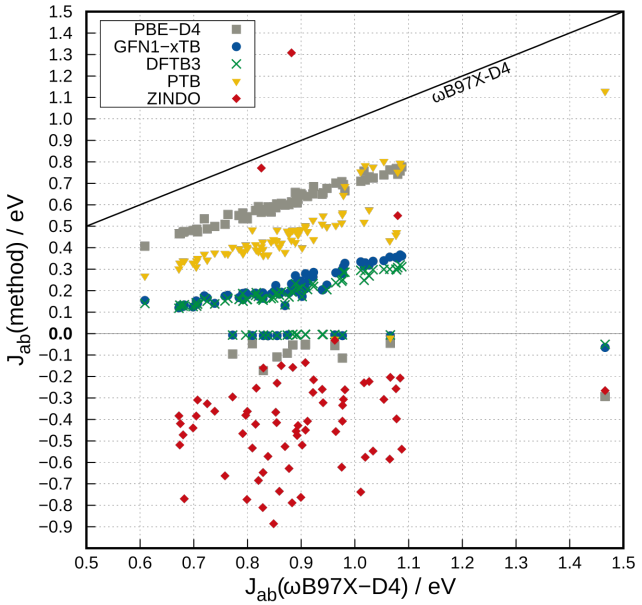

FIG. 2. Correlation plot of different tested methods against ωB97X-D4/TZ2P references, for unscaled J_{ab} in eV of the HAB79 benchmark. The black line denotes perfect correlation with the reference.

Except for ZINDO, all examined methods exhibit a significant correlation with the reference values. Among them, PBE-D4 best reproduces the absolute values, followed by PTB. GFN1-xTB and DFTB3 perform equally, but less well than PTB. While PBE-D4, GFN1-xTB, and DFTB3 exhibit a notable number of outliers near zero, PTB only has two outliers. We will delve into this topic extensively in Tab. I. Generally, PTB and other TB methods adequately describe J_{ab} to derive meaningful $|J_{ab,eff}|$ without sacrificing information, following the aforementioned global scaling with f.

In analogy to Ref. 42 we applied a linear scaling to $|J_{ab,eff}|$ for all examined methods. Notably, this statistical scaling differs from the f=1.921 scaling factor introduced above due to physical reasons. The scaling as proposed by Ref. 42 is based on the inverse of the slope of linear fit functions (b denotes the y-axis intersect and m the slope):

$$X_{scaled} = (X_{unscaled} - b) \cdot \frac{1}{m} \tag{9}$$

The linear fit functions of all examined methods and test sets are given in the SI. Fig. 3 and Tab. I depict the resulting statistical measures.

For the full HAB79 set PTB yields the best results of all examined methods, even better than PBE, closely followed by GFN1-xTB. As noted above, ZINDO performs worst.

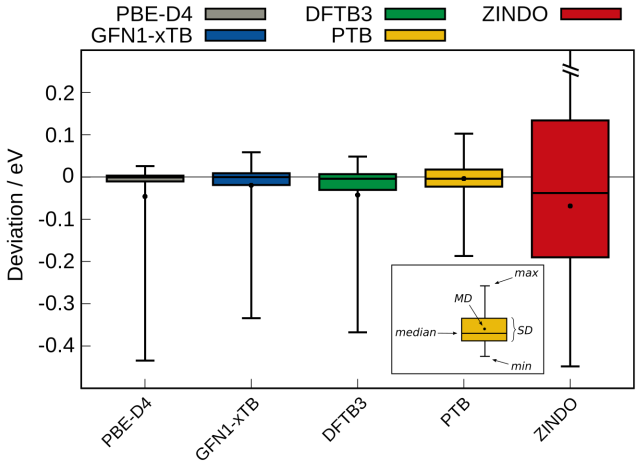

FIG. 3. Statistical measures of different tested methods against ωB97X-D4/TZ2P references, for scaled $|J_{ab,eff}|$ in eV of the HAB79 benchmark with no outliers excluded.

TABLE I. Statistical measures, according to equations 6 to 13, of $|J_{ab,eff}|$ values calculated at different levels of theory for the HAB79 benchmark and compared to ωB97X-D4/TZ2P references. Absolute values are given in meV, relative ones in %. The set does not exclude any outliers. ZINDO values could not be scaled due to missing correlation.

	PBE-D4	GFN1-xTB	DFTB3	PTB	ZINDO
MD	-0.046	-0.020	-0.043	-0.004	0.208
MAD	0.051	0.032	0.053	0.033	0.392
SD	0.112	0.060	0.084	0.049	0.928
relMD	-11.9	-4.8	-10.8	-0.9	59.3
relMAD	13.2	8.0	13.4	7.8	102.3
relSD	28.4	13.9	20.7	11.1	247.3
ρ_S	0.808	0.779	0.699	0.794	-0.175
ρ_P	0.451	0.637	0.55	0.762	-0.139

Another big advantage of PTB, besides its performance, is its robustness. There are only two 2σ-outliers among 79 systems, whereas GFN1-xTB features 11 outliers, PBE 12 outliers, and DFTB3 even 18 outliers. We could not spot any similarities between the mentioned outliers such as sharing a common structural feature or similar drawbacks in the electronic description. Although in principle, outliers could overestimate and underestimate the reference coupling, only the latter occurs, resulting for instance from inaccurate orbital energies, an altered orbital order, a wrong sign of J_{ab} (that may depend on very small contributions of the overlap matrix), or general shortcomings of the DIPRO approach.

The linear scaling improves the tested methods by up to 65% in relMAD or up to 30% in relSD. In general, SQM methods experience a much stronger improvement than PBE, rendering them competitive to GGA DFT, but at a much lower computational cost. Additional statistics for the unscaled values are given in the SI.

B. JAB69

Statistical results for the JAB69 benchmark are presented in Fig. 4 and Tab. II

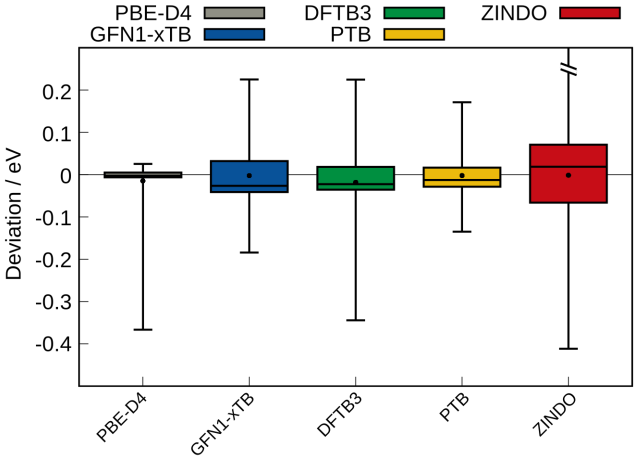

FIG. 4. Statistical measures of different tested methods against ωB97X-D4/TZ2P references, for scaled $|J_{ab,eff}|$ in eV of the JAB69 benchmark with some outliers (e.g. due to convergence issues) or elements excluded due to missing parametrization as mentioned in Tab. II.

TABLE II. Statistical measures, according to equations 6 to 13, of $|J_{ab,eff}|$ values calculated at different levels of theory for the JAB69 benchmark compared to ωB97X-D4/TZ2P references. Absolute values are given in meV, relative ones in %. No. **15** did not converge with PBE and No. **19** not with ZINDO. There were no parameters available for various residues from the CHNOSE subset in DFTB3 (No. **65**, **66**, **69**) and ZINDO (No. **64**, **65**, **66**, **68**, **69** see Figure 1). Accordingly, the respective part of the statistics exclude the mentioned molecules.

	PBE-D4	GFN1-xTB	DFTB3	PTB	ZINDO
MD	-0.015	-0.002	-0.018	-0.002	0.031
MAD	0.022	0.059	0.061	0.039	0.109
SD	0.064	0.077	0.095	0.055	0.168
relMD	-2.865	9.531	-0.242	6.338	55.681
relMAD	8.528	25.147	20.558	17.385	74.368
relSD	22.18	55.94	35.47	38.28	273.05
ρ_S	0.972	0.858	0.819	0.904	0.381
ρ_P	0.879	0.821	0.763	0.896	0.315
no. of molecules	68	69	66	69	63

PBE performs best on the JAB69 benchmark, followed by PTB. ZINDO yields again the worst results, but in contrast to the HAB79 set, the observed correlation allows for linear scaling. This benchmark shows a significantly reduced number of 2σ-outliers compared to the HAB79 benchmark. There are four outliers for PBE, one each for GFN1-xTB and PTB, seven for DFTB3, and nine for ZINDO. Again, outliers share no commonalities, except for No. **15**, **16**, and **17**, that we will discuss in detail. Excluding the outliers from the statistical evaluation has fewer effects than in the HAB79

benchmark; PBE experiences the strongest improvement with 4% in relMAD and 12% in relSD.

The advantage of employing a uniform scaling factor (f) acting on the PTB dimer orbital energies is a significant improvement in many results with minimal additional effort. However, there is a drawback when it comes to certain molecules that are poorly described by such a simplified approach. This applies specifically to ethyne, ethylene, and cyclopropene (**15**, **16**, and **17** in Figure 1), respectively. The scaling factor of 1.921, as described in equations 6 to 8, derived primarily from medium-sized molecules, proves to be too large for these small systems. This scaling factor is size- and distance dependent due to the spatial behavior of molecular orbitals and their overlap.

By increasing the system size of molecules like ethylene and benzene, for instance, through the expansion into homologous rows of polyenes and acenes, the scaling factor converges as the system size grows. Larger systems exhibit optimum scaling factors closer to 2, resulting in smaller final values of $|J_{ab,eff}|$, which arises from the asymptotically decreasing electronic gap. Additional information on this topic can be found in the SI.

The scaling factor is not ideally transferable to non-organic elements such as heavier main group elements or transition metals. Another drawback is the distance dependence of the scaling factor. There are inherent differences in the decrease of $|J_{ab,eff}|$ between SQM and DFT methods due to the minimal basis set of SQM methods lacking long-ranged diffuse functions. As the distance between coupling fragments increases, the scaling factor also increases approximately linear. The scaling factor does not exhibit any angular dependency. Further details can be found in the SI.

Presently, our DIPRO implementation only considers single orbitals for the calculation of coupling integrals, specifically the HOMO/LUMO of each monomer if we are interested in hole/electron couplings and transport properties. This may result in significant deviations in $|J_{ab,eff}|$ when dealing with near-degenerate orbitals or cases where the orbital order has been altered. Additionally, in special linear high-symmetry situations like for ethyne, the local coordinate systems assigned to the individual fragments may differ from the local coordinate system of the less symmetric dimer.

C. Challenging Systems

Relevant molecules for organic electronic applications (e.g., OFETs, photodetectors, OPVs) are merocyanines. Those have been studied and named in the late 40s[59] as dyes and photo-agents; and from the early 80s[60] to today[61] they have been utilized and extensively investigated as OSC materials[62,63]. Recently, merocyanines have been studied for applications in the field of bio-imaging ,[64,65] optical sensors for temperature,[66] pH,[67] or chemicals,[68] photosensitizers in nanomedicine and cancer therapy,[69,70] and antimicrobial drugs.[71,72] The computational investigation of merocyanines is challenging due to their electronic structure, namely the resonance between zwitterionic and neutral structures, and thus strong electron correlation effects. Additionally, most often a single-molecule approach, in contrast to a cluster-aggregate or nano-crystalline approach, is not sufficient to describe all properties of interest. Typically, range-separated hybrid functionals (RSH) and high-level wave function methods like CASSCF/NEVPT2 or CCSD(T) are employed for accurate examinations.[73–75] Notably, the PTB method emulates such RSH behavior and additionally is parameterized to yield good hyperpolarizabilities, which are crucial for describing merocyanines.[76–78] Fig. 5 shows the molecular structures of some merocyanines as well as packing motifs and $|J_{ab,eff}|$ for various SQM methods.

Among the tested SQM methods, ZINDO and PTB show the best agreement with the reference ωB97X-D4/TZ2P, reproducing the order of magnitude as well as the relative order of couplings. Noteworthy, the average coupling of the investigated merocyanines is almost by factor 0.5 lower than the estimated target accuracy of the SQM methods as determined for the HAB79 and JAB69 benchmarks. The very good performance of PTB and ZINDO for the merocyanines is rather surprising. Firstly, merocyanines are dipolar molecules with significant charge delocalization, which is generally challenging for SQM methods to describe accurately. Secondly, the diverse dimer packing motifs, ranging from eclipsed stacking to in-plane coupling and various close dimers (see Fig. 5c), pose a high challenge for SQM to achieve a uniform treatment. Thirdly, the universal scaling factor used in PTB is not tailored to merocyanines. Lastly, the methods perform reasonably over a coupling range of four orders of magnitude, i.e. spanning from 10^{-3} eV to over 10^{0} eV, for most of which they have not been benchmarked. Considering these factors, the remarkable correlation between PTB and ZINDO is exceptional, particularly because ZINDO has previously shown less favorable results in our JAB69 and HAB79 benchmark study, and PTB has occasionally suffered from overscaling (notably, only merocyanine **3a** is overscaled). So far, we were not able to exploit the exact reasons for the good performance of ZINDO for the merocyanines, which is in contrast to the rather poor performance for the benchmarks sets discussed above. Overall, these findings highlight the favorable transferability of the DIPRO@PTB approach to molecular materials with complex/challenging electronic structure and conformational flexibility.

MOFs are relevant and emerging materials in the development of modern organic electronics.[79–81] They are independent supramolecular building blocks that exhibit a high degree of order and can easily be customized for special applications. Furthermore, MOFs use the advantageous electronic properties of metals while only containing a minimal amount of them, whereas merocyanines are purely organic. In the following, we show the calculation of coupling integrals for a large metal organic cage (MOC) with PTB. MOCs are the one-dimensional variant of MOFs. Our test case is shown in Figure 6.

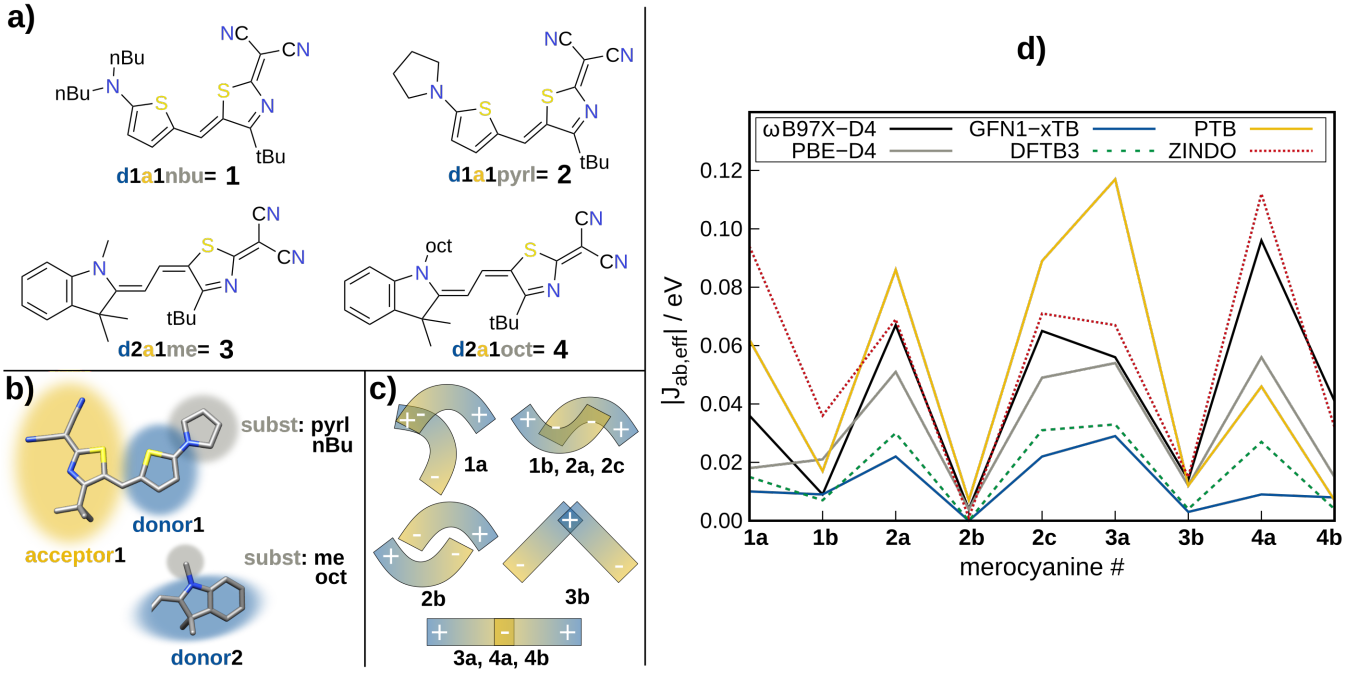

FIG. 5. Panel a): different kinds of merocyanines (1-4) as derived by combination of various donor (d) and acceptor (a) groups. Panel b): molecular structures of donor and acceptor groups, with indication of different substituents, namely: methyl (me), normal-butyl (nBu), octyl (oct) and pyrrolidine (pyrl). Panel c): sketches of possible intermolecular packing motifs. Panel d) coupling integrals $|J_{ab,eff}|$ in eV for different merocyanine dimers at different levels of theory.

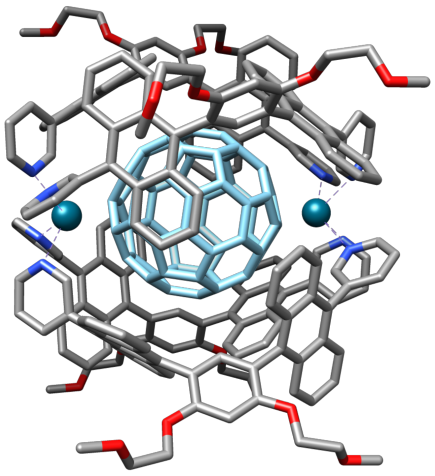

FIG. 6. GFN2-xTB/ALPB($CHCl_3$) optimized structure of the examined MOC[82] . Hydrogens are omitted for clarity, the two displayed metal atoms are Palladium.

The examined MOC is an organic cage constituted of Pd-linked anthracene panels encapsulating a C_{60} fullerene. Such host-guest systems are dominated by non-covalent interactions (NCIs) which are in general difficult to describe as they rely on electron correlation effects. Dispersion corrected DFT and the GFN-xTB methods are able to describe NCI systems reasonably accurate. The $|J_{ab,eff}|$ results for different methods are given in Tab. III.

The coupling integrals computed with the low-level methods exhibit good agreement with the ωB97X-D4 reference, both qualitatively and in terms of magnitude. Unfortunately, it was not possible to test ZINDO due to the absence of parameters for Pd. As previously mentioned, the scaling factor of 1.921 for PTB may not be suitable for extremely large or small systems. Consequently, we also present the unscaled values in this study. It is important to note that the comparability of coupling integrals between different methods relies on the similarity of the underlying molecular orbitals. The degree of orbital delocalization and degeneracy increases with the extension of the π-system. To address this issue, we conducted a manual inspection of the molecular orbitals near the active space and arranged the couplings to maximize the similarity of transfer orbitals. Orbital visualizations are available in the SI (Fig. S5). In terms of describing charge transfer

TABLE III. $|J_{ab,eff}|$ in meV for different methods and different combination of molecular orbitals. h corresponds to the HOMO, h-1 to HOMO-1, and l to LUMO.

orbitals						
cage	C_{60}	ωB97X-D4	PBE-D4	GFN1-xTB	PTB	$PTB_{unscaled}$
h-1	h-1	22	10	13	12	5
h	h-1	60	24	56	79	36
h-1	h	3	8	8	7	3
h	h	23	21	38	57	24
h-1	l	40	155	86	72	33
h	l	434	73	55	639	292
l	l	20	18	68	10	4

integrals, PTB outperforms GFN1-xTB and PBE-D4 due to its partial RSH character. Despite the inherent challenges associated with merocyanines as well as MOCs, such as high correlation effects, large system size, intricate electronics, inclusion of metals, orbital ordering, and near-degeneracy, PTB performs well in describing them.

Approximate computation times on a quadruple core computer range from approximately one minute for GFN1-xTB, around six minutes for PTB, and 30 hours for PBE-D4/TZ2P to over five days for the ωB97X-D4/TZ2P reference.

VI. CONCLUSION AND OUTLOOK

We utilized the recently developed semiempirical PTB method in combination with the dimer projection method DIPRO, to compute intermolecular hole transfer coupling integrals, denoted as $|J_{ab,eff}|$. To enhance the correlation with the reference method ωB97X-D4/TZ2P, we determined a basic scaling factor for PTB, resulting in an improvement of up to 60% for the computed coupling values. Our study involved testing several SQM methods on Blumberger's HAB79 benchmark as well as our newly compiled JAB69 benchmark. The performance of all methods based on tight-binding models was highly satisfactory after scaling, with PTB even surpassing the previously assumed accuracy limit of 100 to 120 meV in MAD for the JAB69 set. Specifically, PTB achieved a MAD of 76 meV, while other tight-binding methods exhibited MAD values around 260 meV and ZINDO showed a MAD of 317 meV. PTB exhibited general robustness against outliers, even slightly outperforming GGA-DFT in this aspect. Additionally, PTB demonstrated the ability to handle heavier main-group elements and transition metals due to its comprehensive parameterization covering all elements. On the other hand, a major drawback of PTB is its need for a system and distance dependent empirical scaling factor. Furthermore, we demonstrated the transferability of our approach to medium-sized merocyanines and large-sized MOCs, both of which are prominent examples in organic electronics. The computational speedup of PTB achieved in calculating $|J_{ab,eff}|$ for a MOC system with 446 atoms, compared to GGA-DFT, is approximately 300-fold. Yet the PTB results are in good agreement with the hybrid-DFT reference. Further improvements for a better treatment of nearly degenerate and partially occupied orbitals with the DIPRO approach are already envisioned.

ACKNOWLEDGMENTS

The authors thank the *German Research Foundation* (DFG) for funding in the framework of *RTG 2591 - Template-Designed Organic Electronics (TIDE)*.

AUTHOR DECLARATIONS

Conflict of interest

The authors have no conflicts to disclose.

AUTHOR CONTRIBUTIONS

J. K. performed the computational analyses. N. G. and D. F. contributed all calculations performed with `Gaussian16`. A. H. conceptualized the work. All authors contributed to rationalize the data and wrote the manuscript.

DATA AVAILABILITY STATEMENT

The data that support the findings of this study are available within the article and its supplementary material. The customized alpha program versions are available from the authors upon request.

[1] R. R. Nazmutdinov and J. Ulstrup, "Retrospective and prospective views of electrochemical electron transfer processes: theory and computations," Atomic-Scale Modelling of Electrochemical Systems , 25–91 (2021).
[2] P. Ramos, M. Mankarious, and M. Pavanello, "A critical look at methods for calculating charge transfer couplings fast and accurately," Practical Aspects of Computational Chemistry IV , 103–134 (2016).
[3] A. Y. Sosorev, "Simple charge transport model for efficient search of high-mobility organic semiconductor crystals," Mater. Des. **192**, 108730 (2020).
[4] H. Dong, X. Fu, J. Liu, Z. Wang, and W. Hu, "25th anniversary article: key points for high-mobility organic field-effect transistors," Adv. Mater. **25**, 6158–6183 (2013).
[5] B. Baumeier, F. May, C. Lennartz, and D. Andrienko, "Challenges for in silico design of organic semiconductors," J. Mater. Chem. **22**, 10971–10976 (2012).
[6] H. Oberhofer, K. Reuter, and J. Blumberger, "Charge transport in molecular materials: An assessment of computational methods," Chem. Rev. **117**, 10319–10357 (2017).
[7] V. Coropceanu, Y. Li, Y. Yi, L. Zhu, and J.-L. Brédas, "Intrinsic charge transport in single crystals of organic molecular semiconductors: A theoretical perspective," MRS Bull. **38**, 57–64 (2013).
[8] S. Giannini and J. Blumberger, "Charge transport in organic semiconductors: the perspective from nonadiabatic molecular dynamics," Acc. Chem. Res. **55**, 819–830 (2022).
[9] V. Coropceanu, J. Cornil, D. A. da Silva Filho, Y. Olivier, R. Silbey, and J.-L. Brédas, "Charge transport in organic semiconductors," Chem. Rev. **107**, 926–952 (2007).
[10] W. Brütting, "Introduction to the physics of organic semiconductors," Physics of organic semiconductors , 1–14 (2005).
[11] H. Bässler and A. Köhler, "Charge transport in organic semiconductors," Unimolecular and Supramolecular Electronics I: Chemistry and Physics Meet at Metal-Molecule Interfaces , 1–65 (2012).
[12] A. Nenashev, J. Oelerich, and S. Baranovskii, "Theoretical tools for the description of charge transport in disordered organic semiconductors," J. Phys. Condens. Matter **27**, 093201 (2015).
[13] S. D. Baranovskii, "Mott lecture: Description of charge transport in disordered organic semiconductors: Analytical theories and computer simulations," Phys. Status Solidi **215**, 1700676 (2018).
[14] N. Gildemeister, G. Ricci, L. Böhner, J. M. Neudörfl, D. Hertel, F. Würthner, F. Negri, K. Meerholz, and D. Fazzi, "Understanding the structural and charge transport property relationships for a variety of merocyanine single-crystals: a bottom up computational investigation," J. Mater. Chem. C **9**, 10851–10864 (2021).

[15] S. Di Motta, E. Di Donato, F. Negri, G. Orlandi, D. Fazzi, and C. Castiglioni, "Resistive molecular memories: influence of molecular parameters on the electrical bistability," J. Am. Chem. Soc. **131**, 6591–6598 (2009).
[16] S. Di Motta, M. Siracusa, and F. Negri, "Structural and thermal effects on the charge transport of core-twisted chlorinated perylene bisimide semiconductors," J. Phys. Chem. C **115**, 20754–20764 (2011).
[17] A. Baggioli, M. Casalegno, G. Raos, L. Muccioli, S. Orlandi, and C. Zannoni, "Atomistic simulation of phase transitions and charge mobility for the organic semiconductor ph-btbt-c10," Chem. Mater. **31**, 7092–7103 (2019).
[18] Y. Mao, A. Montoya-Castillo, and T. E. Markland, "Accurate and efficient dft-based diabatization for hole and electron transfer using absolutely localized molecular orbitals," J. Chem. Phys. **151**, 164114 (2019).
[19] Q. Wu and T. Van Voorhis, "Extracting electron transfer coupling elements from constrained density functional theory," J. Chem. Phys. **125**, 164105 (2006).
[20] C. Schober, K. Reuter, and H. Oberhofer, "Critical analysis of fragment-orbital dft schemes for the calculation of electronic coupling values," J. Chem. Phys. **144**, 054103 (2016).
[21] S. Ghan, C. Kunkel, K. Reuter, and H. Oberhofer, "Improved projection-operator diabatization schemes for the calculation of electronic coupling values," J. Chem. Theor. Comput. **16**, 7431–7443 (2020).
[22] I. Kondov, M. Čížek, C. Benesch, H. Wang, and M. Thoss, "Quantum dynamics of photoinduced electron-transfer reactions in dye- semiconductor systems: First-principles description and application to coumarin 343-tio2," J. Phys. Chem. C **111**, 11970–11981 (2007).
[23] Z. Futera and J. Blumberger, "Electronic couplings for charge transfer across molecule/metal and molecule/semiconductor interfaces: Performance of the projector operator-based diabatization approach," J. Phys. Chem. C **121**, 19677–19689 (2017).
[24] P. Ramos, M. Papadakis, and M. Pavanello, "Performance of frozen density embedding for modeling hole transfer reactions," J. Phys. Chem. B **119**, 7541–7557 (2015).
[25] R. J. Cave and M. D. Newton, "Generalization of the mulliken-hush treatment for the calculation of electron transfer matrix elements," Chem. Phys. Lett. **249**, 15–19 (1996).
[26] H. Ren, M. R. Provorse, P. Bao, Z. Qu, and J. Gao, "Multistate density functional theory for effective diabatic electronic coupling," J. Phys. Chem. Lett. **7**, 2286–2293 (2016).
[27] F. Gajdos, S. Valner, F. Hoffmann, J. Spencer, M. Breuer, A. Kubas, M. Dupuis, and J. Blumberger, "Ultrafast estimation of electronic couplings for electron transfer between π-conjugated organic molecules," J. Chem. Theor. Comput. **10**, 4653–4660 (2014).
[28] C.-I. Wang, I. Joanito, C.-F. Lan, and C.-P. Hsu, "Artificial neural networks for predicting charge transfer coupling," J. Chem. Phys. **153**, 214113 (2020).
[29] R. Hafizi, J. Elsner, and J. Blumberger, "Ultrafast electronic coupling estimators: Neural networks versus physics-based approaches," J. Chem. Theor. Comput. (2023).
[30] B. Baumeier, J. Kirkpatrick, and D. Andrienko, "Density-functional based determination of intermolecular charge transfer properties for large-scale morphologies," Phys. Chem. Chem. Phys. **12**, 11103–11113 (2010).
[31] H. Kitoh-Nishioka and K. Ando, "Charge-transfer matrix elements by fmo-lcmo approach: Hole transfer in dna with parameter tuned range-separated dft," Chem. Phys. Lett. **621**, 96–101 (2015).
[32] A. Aggarwal, V. Vinayak, S. Bag, C. Bhattacharyya, U. V. Waghmare, and P. K. Maiti, "Predicting the dna conductance using a deep feedforward neural network model," J. Chem. Inf. Model. **61**, 106–114 (2020).
[33] A. Pal, L. K. Wen, C. Y. Jun, I. Jeon, Y. Matsuo, and S. Manzhos, "Comparative density functional theory–density functional tight binding study of fullerene derivatives: effects due to fullerene size, addends, and crystallinity on band structure, charge transport and optical properties," Phys. Chem. Chem. Phys. **19**, 28330–28343 (2017).
[34] T. Nematiaram, D. Padula, A. Landi, and A. Troisi, "On the largest possible mobility of molecular semiconductors and how to achieve it," Adv. Func. Mater. **30**, 2001906 (2020).
[35] A. Troisi and G. Orlandi, "Dynamics of the intermolecular transfer integral in crystalline organic semiconductors," J. Phys. Chem. A **110**, 4065–4070 (2006).
[36] H. Kitoh-Nishioka, K. Welke, Y. Nishimoto, D. G. Fedorov, and S. Irle, "Multiscale simulations on charge transport in covalent organic frameworks including dynamics of transfer integrals from the fmo-dftb/lcmo approach," J. Phys. Chem. C **121**, 17712–17726 (2017).
[37] A. Landi, A. Peluso, and A. Troisi, "Quantitative prediction of the electromechanical response in organic crystals," Adv. Mater. **33**, 2008049 (2021).
[38] Z.-F. Yao, Y.-Q. Zheng, J.-H. Dou, Y. Lu, Y.-F. Ding, L. Ding, J.-Y. Wang, and J. Pei, "Approaching crystal structure and high electron mobility in conjugated polymer crystals," Adv. Mater. **33**, 2006794 (2021).
[39] S. Grimme, M. Müller, and A. Hansen, "A non-self-consistent tight-binding electronic structure potential in a polarized double-ζ basis set for all spd-block elements up to z= 86," The Journal of Chemical Physics **158** (2023).
[40] A. Kubas, F. Gajdos, A. Heck, H. Oberhofer, M. Elstner, and J. Blumberger, "Electronic couplings for molecular charge transfer: benchmarking cdft, fodft and fodftb against high-level ab initio calculations. ii," Phys. Chem. Chem. Phys. **17**, 14342–14354 (2015).
[41] A. Kubas, F. Hoffmann, A. Heck, H. Oberhofer, M. Elstner, and J. Blumberger, "Electronic couplings for molecular charge transfer: Benchmarking cdft, fodft, and fodftb against high-level ab initio calculations," J. Chem. Phys. **140**, 104105 (2014).
[42] O. G. Ziogos, A. Kubas, Z. Futera, W. Xie, M. Elstner, and J. Blumberger, "Hab79: A new molecular dataset for benchmarking dft and dftb electronic couplings against high-level ab initio calculations," J. Chem. Phys. **155**, 234115 (2021).
[43] H. Kitoh-Nishioka and K. Ando, "Calculation of charge-transfer electronic coupling with nonempirically tuned range-separated density functional," J. Phys. Chem. C **123**, 11351–11361 (2019).
[44] A. Pershin and P. G. Szalay, "Improving the accuracy of the charge transfer integrals obtained by coupled cluster theory, mbpt (2), and tddft," J. Chem. Theor. Comput. **11**, 5705–5711 (2015).
[45] M. Pavanello, T. Van Voorhis, L. Visscher, and J. Neugebauer, "An accurate and linear-scaling method for calculating charge-transfer excitation energies and diabatic couplings," J. Chem. Phys. **138**, 054101 (2013).
[46] J.-D. Chai and M. Head-Gordon, "Long-range corrected hybrid density functionals with damped atom–atom dispersion corrections," Phys. Chem. Chem. Phys. **10**, 6615–6620 (2008).
[47] E. Caldeweyher, S. Ehlert, A. Hansen, H. Neugebauer, S. Spicher, C. Bannwarth, and S. Grimme, "A generally applicable atomic-charge dependent london dispersion correction," J. Chem. Phys. **150**, 154122 (2019).
[48] D. P. Chong, E. Van Lenthe, S. Van Gisbergen, and E. J. Baerends, "Even-tempered slater-type orbitals revisited: From hydrogen to krypton," J. Comp. Chem. **25**, 1030–1036 (2004).
[49] J. P. Perdew, K. Burke, and M. Ernzerhof, "Generalized gradient approximation made simple," Phys. Rev. Lett. **77**, 3865 (1996).
[50] M. C. Zerner, "Reviews in computational chemistry," p. 313-365, KB Lipkowitz, DB Boyd Eds., VCH Publishers, Inc (2007).
[51] M. Gaus, Q. Cui, and M. Elstner, "Dftb3: Extension of the self-consistent-charge density-functional tight-binding method (scc-dftb)," J. Chem. Theor. Comput. **7**, 931–948 (2011).
[52] M. Kubillus, T. Kubar, M. Gaus, J. Rezac, and M. Elstner, "Parameterization of the dftb3 method for br, ca, cl, f, i, k, and na in organic and biological systems," J. Chem. Theor. Comput. **11**, 332–342 (2015).
[53] Available upon request.
[54] Available upon request.
[55] M. Frisch, G. Trucks, H. Schlegel, G. Scuseria, M. Robb, J. Cheeseman, G. Scalmani, V. Barone, G. Petersson, H. Nakatsuji, *et al.*, "Gaussian 16 revision c. 01. 2016; gaussian inc," Wallingford CT **421** (2016).
[56] Available upon request.
[57] G. Te Velde, F. M. Bickelhaupt, E. J. Baerends, C. Fonseca Guerra, S. J. van Gisbergen, J. G. Snijders, and T. Ziegler, "Chemistry with adf," J. Comp. Chem. **22**, 931–967 (2001).
[58] G. Te Velde, F. Bickelhaupt, E. Baerends, et. al., "`ADF 2020.102`, SCM", Theoretical Chemistry - Vrije Universiteit Amsterdam. `http://www.scm.com`.
[59] L. Brooker, G. Keyes, R. Sprague, R. VanDyke, E. VanLare, G. VanZandt, F. White, H. Cressman, and S. Dent Jr, "Color and constitution. x. 1 absorption of the merocyanines2," J. Am. Chem. Soc. **73**, 5332–5350 (1951).
[60] G. Chamberlain, P. Cooney, and S. Dennison, "Photovoltaic properties of merocyanine solid-state photocells," Nature **289**, 45–47 (1981).
[61] H. Bürckstümmer, N. M. Kronenberg, M. Gsänger, M. Stolte, K. Meerholz, and F. Würthner, "Tailored merocyanine dyes for solution-processed bhj

solar cells," J. Mater. Chem. **20**, 240–243 (2010).
[62]F. Würthner and K. Meerholz, "Systems chemistry approach in organic photovoltaics," Chem. Eur. J. **16**, 9366–9373 (2010).
[63]A. Liess, L. Huang, A. Arjona-Esteban, A. Lv, M. Gsänger, V. Stepanenko, M. Stolte, and F. Würthner, "Organic thin film transistors based on highly dipolar donor–acceptor polymethine dyes," Adv. Func. Mater. **25**, 44–57 (2015).
[64]C. J. MacNevin, D. Gremyachinskiy, C.-W. Hsu, L. Li, M. Rougie, T. T. Davis, and K. M. Hahn, "Environment-sensing merocyanine dyes for live cell imaging applications," Bioconjugate Chem. **24**, 215–223 (2013).
[65]E. M. Santos, T. Berbasova, W. Wang, R. E. Salmani, W. Sheng, C. Vasileiou, J. H. Geiger, and B. Borhan, "Engineering of a red fluorogenic protein/merocyanine complex for live-cell imaging," Chem. Bio. Chem. **21**, 723–729 (2020).
[66]Y. Shiraishi, M. Itoh, and T. Hirai, "Thermal isomerization of spiropyran to merocyanine in aqueous media and its application to colorimetric temperature indication," Phys. Chem. Chem. Phys. **12**, 13737–13745 (2010).
[67]F. L. Coelho, R. da Costa Duarte, C. de Ávila Braga, J. M. Toldo, P. F. B. Gonçalves, F. da Silveira Santos, and F. S. Rodembusch, "Benzothiazole merocyanine dyes as middle ph optical sensors," Dyes Pigm. **176**, 108193 (2020).
[68]H. Hisamoto, H. Tohma, T. Yamada, K.-i. Yamauchi, D. Siswanta, N. Yoshioka, and K. Suzuki, "Molecular design, characterization, and application of multi-information dyes for multi-dimensional optical chemical sensing. molecular design concepts of the dyes and their fundamental spectral characteristics," Anal. Chim. Acta **373**, 271–289 (1998).
[69]H. Shindy, A. Khalafalla, M. Goma, and A. Eed, "Synthesis, photosensitization and antimicrobial activity evaluation of some novel merocyanine dyes," Chem. Int. **2**, 114–120 (2016).
[70]M. R. Detty, S. L. Gibson, and S. J. Wagner, "Current clinical and preclinical photosensitizers for use in photodynamic therapy," J. Med. Chem. **47**, 3897–3915 (2004).
[71]F. Sieber, J. M. O'Brien, G. J. Krueger, S. L. Schober, W. H. Burns, S. J. Sharkis, and L. L. Sensenbrenner, "Antiviral activity of merocyanine 540," Photochem. Photobiol. **46**, 707–711 (1987).
[72]H.-Y. Lin, C.-T. Chen, and C.-T. Huang, "Use of merocyanine 540 for photodynamic inactivation of staphylococcus aureus planktonic and biofilm cells," Appl. Environ. Microbiol. **70**, 6453–6458 (2004).
[73]B. Tirri, G. Mazzone, A. Ottochian, J. Gomar, U. Raucci, C. Adamo, and I. Ciofini, "A combined monte carlo/dft approach to simulate uv-vis spectra of molecules and aggregates: Merocyanine dyes as a case study," J. Comp. Chem. **42**, 1054–1063 (2021).
[74]C. Brückner, C. Walter, M. Stolte, B. Braida, K. Meerholz, F. Würthner, and B. Engels, "Structure–property relationships for exciton and charge reorganization energies of dipolar organic semiconductors: A combined valence bond self-consistent field and time-dependent hartree-fock and dft study of merocyanine dyes," J. Phys. Chem. C **119**, 17602–17611 (2015).
[75]L. Lescos, S. P. Sitkiewicz, P. Beaujean, M. Blanchard-Desce, B. Champagne, E. Matito, and F. Castet, "Performance of dft functionals for calculating the second-order nonlinear optical properties of dipolar merocyanines," Phys. Chem. Chem. Phys. **22**, 16579–16594 (2020).
[76]Y. Siqueira, M. L. Lyra, T. N. Ramos, B. Champagne, and V. Manzoni, "Unveiling the relationship between structural and polarization effects on the first hyperpolarizability of a merocyanine dye," J. Chem. Phys. **156**, 014305 (2022).
[77]M. E. Reish, A. J. Kay, A. Teshome, I. Asselberghs, K. Clays, and K. C. Gordon, "Testing computational models of hyperpolarizability in a merocyanine dye using spectroscopic and dft methods," J. Phys. Chem. A. **116**, 5453–5463 (2012).
[78]F. Castet, M. Blanchard-Desce, F. Adamietz, Y. M. Poronik, D. T. Gryko, and V. Rodriguez, "Experimental and theoretical investigation of the first-order hyperpolarizability of octupolar merocyanine dyes," Chem. Phys. Chem. **15**, 2575–2581 (2014).
[79]M. D. Allendorf, A. Schwartzberg, V. Stavila, and A. A. Talin, "A roadmap to implementing metal–organic frameworks in electronic devices: challenges and critical directions," Chem. Eur. J. **17**, 11372–11388 (2011).
[80]M. Souto, K. Strutyński, M. Melle-Franco, and J. Rocha, "Electroactive organic building blocks for the chemical design of functional porous frameworks (mofs and cofs) in electronics," Chem. Eur. J. **26**, 10912–10935 (2020).
[81]M. Wang, R. Dong, and X. Feng, "Two-dimensional conjugated metal–organic frameworks (2d c-mofs): chemistry and function for moftronics," Chem. Soc. Rev. **50**, 2764–2793 (2021).
[82]N. Kishi, Z. Li, K. Yoza, M. Akita, and M. Yoshizawa, "An m2l4 molecular capsule with an anthracene shell: encapsulation of large guests up to 1 nm," J. Am. Chem. Soc. **133**, 11438–11441 (2011).